Article:
Abuserwal, A.F., Elizondo Luna, E.M., Goodall, R. et al. (1 more author) (2017) The effective thermal conductivity of open cell replicated aluminium metal sponges. International Journal of Heat and Mass Transfer, 108 (B). pp. 1439-1448. ISSN 0017-9310

https://doi.org/10.1016/j.ijheatmasstransfer.2017.01.023

The Effective Thermal Conductivity of Open Cell Replicated Aluminium Metal Sponges

Ahmed F Abuserwal[1], Erardo M Elizondo Luna[2], Russell Goodall[2], Robert Woolley[1]

[1] Department of Mechanical Engineering

[2] Department of Materials Science & Engineering

University of Sheffield, Sheffield,

Mappin Street Sheffield S1 3JD, UK

Highlights

Measurements of the effective thermal conductivity of open cell aluminium porous sponges.

Samples manufactured using the replication technique with porosity of 0.57 to 0.77 and pore sizes between 0.7 to 2.4 mm

An empirical correlation was derived for sintered porous materials with porosities ranging from 0.5 to 1.0.

Abstract

The effective thermal conductivity of aluminium open cell porous materials has been tested using the steady state method. The materials were manufactured using the replication technique producing samples of porosity ranging from 0.57 to 0.77 and pore sizes between 0.7 to 2.4 mm. The effective thermal conductivity was found to decrease with increasing porosity, but there was no notice influence of pore size. The results were found to be in general agreement with similar measurements found in the literature. The differences observed were attributed to the thickness and structure of the material in the matrix. Overall there was better agreement between the experiments than for the correlations and analytical expressions presented in the literature. An empirically derived correlation was obtained for sintered porous materials with porosities ranging from 0.5 to 1.0.

Key words

Porous metals, effective thermal conductivity, experiments, correlation

Nomenclature

A	cross sectional area
m	mass
V	volume
d_p	diameter
K	thermal conductivity
L_1	upper aluminium block thickness
L_2	lower aluminium block thickness
L_s	sample thickness
Q_I	upper block heat transfer rate
Q_{II}	lower block heat transfer rate
Q_s	sample heat transfer rate
D_o	insulation outer diameter
D	aluminium block diameter
D_{st}	struts thickness
d_{lu}	node thickness
T	temperature
Q_{Loss}	heat loss to outside
ΔT	temperature difference

Greek symbols

ε	porosity
ρ	density

Abbreviations

ETC & K_{eff}	effective thermal conductivity
PPI	Pores Per Inch
TPS	transient plan source
NaCl	sodium chloride
V.S	very small samples
S	small samples
M	medium samples
L	large samples

Subscript

s	sample
sol	solid
t	total
Al	aluminium
p	pore

o	outer
i	inner
Av	average
eff	effective
in	insulation

1. Introduction

Metal foams and sponges are versatile materials (see for example [1] and [2]) that have a number of thermal applications in regenerators, air-conditioning systems, gas turbines, electronic cooling and chemical reactors[3-6]. Their main advantage is their high specific area which enhances the heat transfer and permits miniaturization of the thermal system. Moreover, their geometric construction enhances flow mixing as a result of their tortuous pathways [5, 7]. As a result, they have attracted considerable attention in recent times. The thermal conductivity is an important parameter for such applications and can be accessed by approximating the porous material as an equivalent homogenous medium. When heat, driven by a temperature gradient, flows by conduction in this situation, the use of the Fourier law implies knowledge of the effective thermal conductivity *(ETC)*.

Heat exchange in porous structures is complex as it takes place in two phases. There is a network of solid ligaments of generally high thermal conductivity and a fluid with lower thermal conductivity [8, 9]. The principle process of heat transfer in non-flowing fluid saturated media is conduction through both the solid and fluid phases. However, convection and radiation cannot necessarily be neglected in all cases [7, 10].

In such situations, the effective thermal conductivity, *ETC*, is no longer a property of a single material but depends on both the solid and fluid material properties, and also the structure of the porous medium; e.g. its porosity and pore size. A further problem with these materials is that the repeatability of the morphology is not constant, even when the same manufacturing conditions are employed, resulting in an inherent scatter in the material properties unless very large samples are tested [5, 11, 12].

Porous materials are generally characterised using their porosity and pore size. The porosity (ε, the inverse of the amount of solid material) is well defined and easily measured, it only requires that the mass and volume are known. The effective thermal conductivity has been found to be highly sensitive to the porosity, increasing as the porosity decreases [5-8, 13-15]. The effect of pore size on *ETC* is less significant, and generally no noticeable effect of pore size has been reported [5, 8, 9, 15], provided the pore size is below a

certain value shown to be 4 mm diameter in closed cell polymer foams which is sufficient to suppress convection [3, 16, 17]. Although it can be demonstrated that the pore size has little direct influence on *ETC*, the pore size will influence the foam fabrication process, and by establishing limits on what foams may actually be produced (there are usually upper and lower size limits). To this extent, pore size can affect the *ETC* [12, 18]. The pore size itself is additionally not well defined as measures including both average pore diameters and Pores Per Inch (*PPI*) are presented in the literature. Conversion between the these measures is also subject to ambiguity [3, 17].

There have been a number of attempts to provide theoretical approaches (often based on a simplified unit cell structure) and empirical correlations to predict *ETC* in porous materials. The models require some assumptions to be made; relating to the topology, the arrangement of the solid and fluid phases (whether in series or parallel) and the repeatability of distribution of the unit cells [19, 20]. There are many different production techniques available [3, 17]. Different production technique and the type of material have an effect in terms of strut shape and size, and distribution of the pores [21], as well as the base material from which the porous metal is made. However, these general approaches have not been successful in predicting the *ETC* of most open celled metal sponges with accuracy. Strategies that go beyond simplified unit cell structures have been explored, for example, by analysing the real foam structure obtained from 3D computed tomography [12] to observe its effects on the *ETC*. This can support the development of more accurate generic correlations [10, 12, 18], but is limited by the small volumes of foams that can be investigated in this way. A review of the wide range of theoretical and empirical approaches for porous metals found that each model defines a specific morphology and is hence of limited applicability to other types [11, 12, 18]. This is discussed in more detail later in this work.

Both steady state and transient techniques may be used to measure the thermal conductivity of complex materials [5, 6, 8-10, 15, 22, 23]. The transient method was first demonstrated by Gustafsson et al [24] in 1979 for *ETC* measurements of insulating materials. The most common type of transient measurement is the Transient Plane Source technique (TPS) [25, 26], where a single element acts as both temperature sensor and heat source . It has been widely used to measure the *ETC* of porous materials [6, 12, 23]. The TPS element is positioned between two samples with similar characteristics and measures the instantaneous temperature gradient with time [6, 25, 26]. The main advantages of this approach are that the tests are easy and rapid, and it is possible to measure a wide range of thermal conductivities [6, 10]. The

analysis can be complex and quantification of uncertainty difficult [10]. Special care of the thermal contact resistance in terms of surface roughness and contact pressure is required [6].

There are a number of steady state methods which can be used to measure the thermal conductivity [10]. The basic principle of a steady state method is to measure the temperature gradient along a sample length under steady state conditions. The rate of heat transfer is obtained by measuring the temperature difference across a known reference material [9, 27] or the dissipated heat from the temperature change in a water bath [5]. The main advantages of this method are the simplicity of the evaluation technique, good precision and accuracy and the opportunity to conduct unidirectional measurements [10]. Whilst the main disadvantages are the long times required to achieve steady state conditions, complicated instrumental procedure and the potential difficulties due to thermal contact (which can be especially challenging for a porous matrix [10]).

The primary objective of the experimental work reported here was to measure the effective thermal conductivity of open celled aluminium porous metals with different pore densities and the assessment of models and empirical correlations at a lower range of porosities than previously available. In this study a comparative steady state method was used where heat transfer through the porous media is allowed to become constant, permitting the application of Fourier's law [5, 9, 27]. Most previous investigations on open celled metal sponges have examined materials with high porosity ($\varepsilon > 0.9$). This study aims to experimentally measure the *ETC* at a lower range of porosities ($0.57 < \varepsilon < 0.77$) using aluminium sponges manufactured using the replication method [28]. The fluid was air. Four different pore sizes (based on the size of the particles used to manufacture the material) were tested, ranging from 0.8 to 2.1 mm in average diameter. The validity of available models and correlations in the literature was tested.

2. Metal samples

Sixty nine aluminium sponge samples were produced by the replication method, using gas pressure to force liquid aluminium to permeate a preform of salt (NaCl) particles, with the salt being washed out once the aluminium has solidified. A detailed description of the method and equipment used can be found in [29]. The porous metal samples were made in four different pore sizes, classified by the average diameter of the infiltration salt particles used in

manufacturing, as this has a direct relationship with the size of the pores. The shape and distribution of the pores is random in nature reflecting the shape and packing of the salt crystals. Pore sizes ranges were (0.71-1.0 mm, 1.0-1.2 mm, 1.4-1.8 mm and 2.0-2.4 mm). The samples were manufactured from 99.9% pure aluminium, the average sample diameter was 50.1 mm with thickness ranging from 22 mm to 30 mm. The aluminium thermal conductivity was taken to be 205 W/m.K and fluid phase was air with thermal conductivity 0.0266 W/m.K at 32^{o}C [30]. The porosity (ε) of the samples (the void volume divided by the total volume) was found by measuring the sample mass (m_s) and volume (V_t), and calculating what the total mass of the sample would be if where solid (m_t) [22, 31, 32]

$$\varepsilon = \frac{\rho_{sol} - m_s/V_t}{\rho_{sol} - \rho_{air}} \qquad 2.1$$

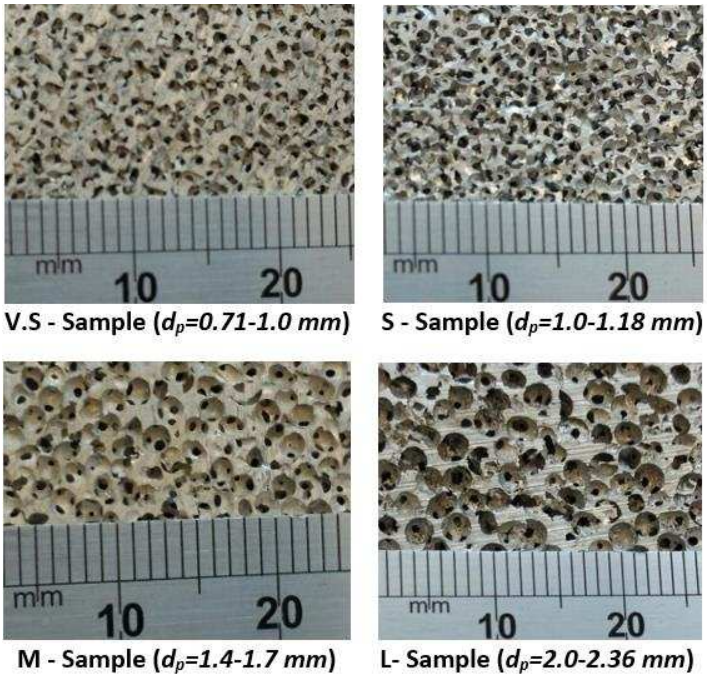

Figure 1. Low magnification images of the surface appearance of different pore size samples.

The samples' porosities ranged from 0.57 to 0.77 with different pore sizes and uncertainties less than 0.7%. Shown in Figure 1 are the photos of tested samples for different pore sizes. The sample specifications and effective thermal conductivity results are given in Table 1.

Table 1 Geometrical parameters and experimental results of effective thermal conductivity of aluminium metal sponge samples

Sample [A]	ε	K_{eff} W/m.K	Sample [B]	ε	K_{eff} W/m.K	Sample [C]	ε	K_{eff} W/m.K	Sample [C]	ε	K_{eff} W/m.K	Sample [D]	ε	K_{eff} W/m.K
V.S-1	0.7225	21.45	S-1	0.6301	33.15	M-1	0.6103	36.92	M-17	0.7578	21.22	L-1	0.6158	34.17
V.S-2	0.6962	23.67	S-2	0.6272	33.20	M-2	0.6205	35.80	M-18	0.6853	28.58	L-2	0.5943	40.00
V.S-3	0.666	24.34	S-3	0.6184	36.76	M-3	0.6323	33.29	M-19	0.6816	25.42	L-3	0.6371	33.39
V.S-4	0.659	35.98	S-4	0.6272	35.00	M-4	0.6425	32.31	M-20	0.7170	22.67	L-4	0.6116	37.80
V.S-5	0.6822	31.96	S-5	0.6960	26.37	M-5	0.6308	33.79	M-21	0.6919	23.90	L-5	0.6235	31.85
V.S-6	0.6595	27.61	S-6	0.6992	25.71	M-6	0.6000	37.62	M-22	0.7091	26.01	L-6	0.6207	31.10
V.S-7	0.6643	27.34	S-7	0.7302	21.11	M-7	0.6369	32.19	M-23	0.7306	24.55	L-7	0.6612	29.54
V.S-8	0.715	26.63	S-8	0.6683	29.73	M-8	0.6415	31.22	M-24	0.6896	26.38	L-8	0.6492	31.60
V.S-9	0.665	36.32	S-9	0.6680	27.93	M-9	0.6168	36.23	M-25	0.7018	28.20	L-9	0.6491	33.44
V.S-10	0.643	35.3	S-10	0.6990	23.39	M-10	0.6922	28.93	M-26	0.6937	24.84	L-10	0.6974	25.01
V.S-11	0.680	31	S-11	0.7246	22.26	M-11	0.6902	27.30	M-27	0.5750	42.21	L-11	0.7075	24.65
V.S-12	0.679	28	S-12	0.7107	22.04	M-12	0.6766	28.00				L-12	0.7224	26.04
			S-13	0.6770	30.38	M-13	0.7628	19.90				L-13	0.6929	25.83
			S-14	0.7227	26.50	M-14	0.7796	16.60				L-14	0.6907	27.24
						M-15	0.7527	20.00				L-15	0.7222	21.27
						M-16	0.6317	30.00				L-16	0.7311	22.44

A- Very small pore size samples (d_p=0.7-1.0 mm & *PPI*=20-25)

B- Small pore size samples (d_p=1.0 -1.2 mm & *PPI*=15-20)

C- Medium pore size samples (d_p=1.4 -1.7 mm & *PPI*=10-15)

D- Large pore size samples (d_p=2.0 - 2.4 mm & *PPI*=5-10)

3. Experimental Apparatus and Effective Thermal Conductivity Calculations

Shown in Figure 1 is a schematic diagram of the apparatus used to estimate the effective thermal conductivity in this study. The method used is comparative steady state which is widely employed to measure the *ETC* of porous materials, e.g. [5, 9, 27].

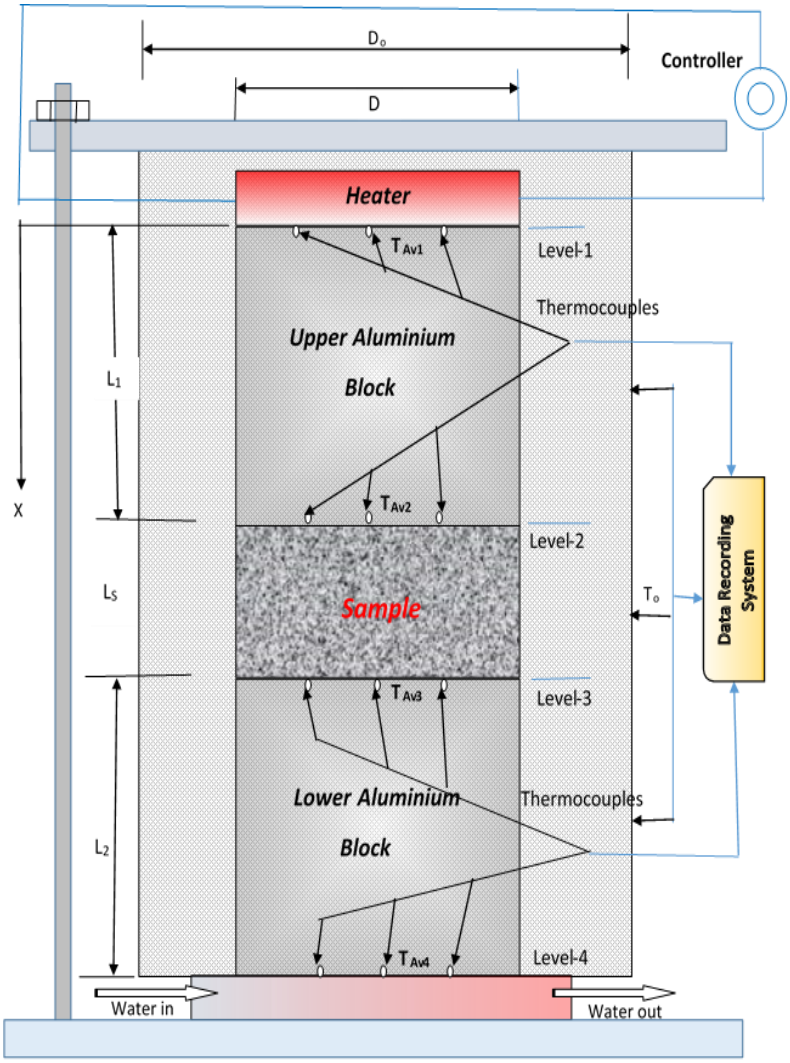

Figure 1. A schematic diagram of a comparative steady state technique used for effective thermal conductivity measurements.

The test rig consisted of a heater, aluminium blocks placed above and below the sample, a cold source (in this case a water bath) and insulation. A 100 W electric resistance heater supplied a uniform heat flux and was in thermal contact with the upper aluminium block, which acted as the upper heat flux meter. The lower block, placed on a bath of flowing cooled water, was the lower heat flux meter. The thickness (L_1=L_2) of both aluminium blocks was 50 mm and their diameter was equal to the average diameter of the tested samples (D=50.1 mm). Both the chiller and heater temperatures were

adjustable. All parts of the rig were contained within polyisocyanurate rigid foam insulation with a thermal conductivity of 0.022 W/m.K to minimise heat loss to the surroundings [33].

The sample was located between the aluminium blocks, whose surfaces were polished and thermal grease was applied to reduce the thermal contact resistance at the join. Twelve K-type thermocouples (diameter 1.5 mm) were used to record the temperatures at four positions. Three grooves were drilled to insert thermocouples at each contact face in different radial locations to measure the temperature profile at the surfaces. Measurement of the temperatures here, rather than away from the contact areas, was necessitated by the rig design. The thermocouples were calibrated against a mercury thermometer using boiling water and melting ice as reference levels. The deviation between thermocouples and mercury thermometer did not exceed ±0.2°C. Errors due to thermocouples' contact and location are included in the overall accuracy assessed later.

The rig was supported by two aluminium plates located at the top and bottom, bolted together to achieve a good contact between all surfaces. The temperatures at four different heights were recorded every second by two USB TC-08 Thermocouple Data Loggers. At each height three temperatures were recorded to determine the radial temperature distribution which was found to be less than 2.5%. For the majority of measurements reported here the heater was set to 50°C and circulating water from the chiller at 5°C. The contribution of radiation heat transfer between the adjacent layers inside the sample and between the contact surfaces of the sample and the block was found less than 1% and 0.5% respectively for other experiments on porous metals [14, 34]. In order to find the heat loss through the insulation, the temperature was measured in three places at the insulation outer surface. After achieving steady state (~ 1000 s), temperatures were recorded for 25 minutes and the average taken over this period. Examples of the experimental readings is shown in Figure 3.

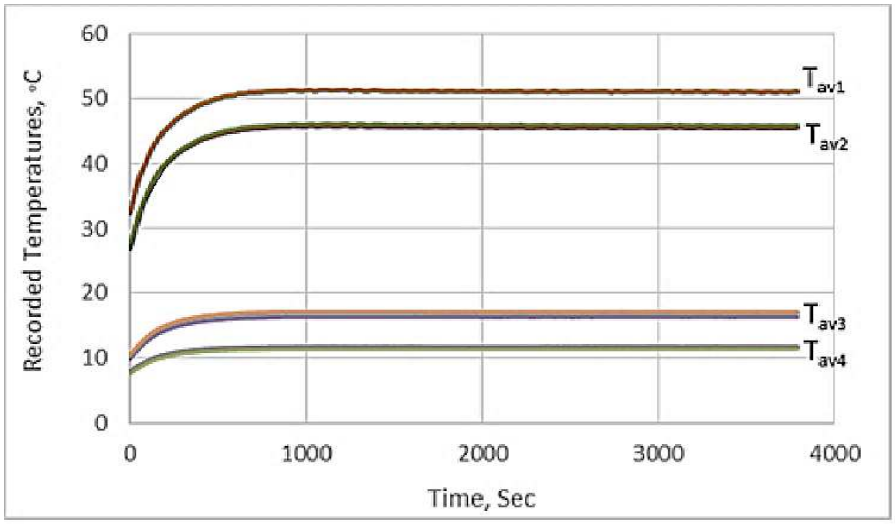

Figure 3 experimentally recorded temperatures with time for a single test. Positions 1 and 2 refer to either side of the heated aluminium block and positions 3 and 4 refer to the water cooled block.

The one dimensional heat transfer problem was applied in the upper and lower aluminium blocks and the porous metal sample, when at thermal equilibrium (steady state). The average of the heat transfer rates in the upper and lower aluminium blocks was used to obtain the *ETC* of the porous material sample.

Assuming no radial conduction, radiation or convection heat transfer the heat flux is a function of the sample thickness only. The heat balance equations through the upper and lower blocks are:

$$Q_I = -A.K_{AL}\frac{\partial T}{\partial X} = A.K_{Al}\frac{(T_{Av1}-T_{Av2})}{L_1} \qquad 3.1$$

$$Q_{II} = -A.K_{AL}\frac{\partial T}{\partial X} = A.K_{Al}\frac{(T_{Av3}-T_{Av4})}{L_2} \qquad 3.2$$

The heat loss (Q_{loss}) to the environment was estimated by applying the heat equation through the insulation material. The inner side temperature of the insulation (T_i) was assessed by the average of outer temperatures at all levels:

$$Q_{Loss} = \frac{2\pi L_s K_{in}(T_i-T_o)}{\ln(D_o/D)} \qquad 3.3$$

where:

A= cross sectional area of the sample and aluminium block, m^2

K_{AL}= thermal conductivity of aluminium block material, W/m.K

K_{in}= thermal conductivity of insulation material, W/m.K

L_1, L_2 and L_s are the lengths of the upper block, lower block and sample respectively.

The heat flow through the sample is the average of both heat flow through the upper and lower aluminium blocks corrected by subtracting the heat loss to the surroundings:

$$Q_s = \frac{Q_I + Q_{II}}{2} - Q_{Loss} \qquad 3.4$$

The effective thermal conductivity can be found by applying the energy balance equation through the sample as

$$K_{eff} = Q_s . L_s / A(T_{Av2} - T_{Av3}) \qquad 3.5$$

The experiment was repeated by rotating the samples, and the average value of the results obtained is reported. The results and geometrical specifications of the tested porous aluminium samples were given in Tables 1. To calibrate the thermal conductivity measurements, three solid materials of known characteristics (aluminium, brass and steel) were also tested. Their thermal conductivities were found to be within 5% of the published values [30].

Whilst in this analysis natural convection was assumed to be negligible previous workers have demonstrated that it can contribute to heat transfer in this type of test [9]. To test for its impact the rig was rotated such that the heat source was below the sample. This configuration has been shown to encourage air movement within the pores due to buoyancy forces [9]. Natural convection depends on the temperature, and so measurements were performed for a range of heater temperatures; the results are shown in Fig. 4 for large pore size samples. The effective thermal conductivity increased with temperature, as might be expected as both the thermal conductivity of air and aluminium increase with temperature. However, once these factors were taken into account, it was found that the relative contribution of convection also increased by ~1% for an 8°C rise in the air temperature.

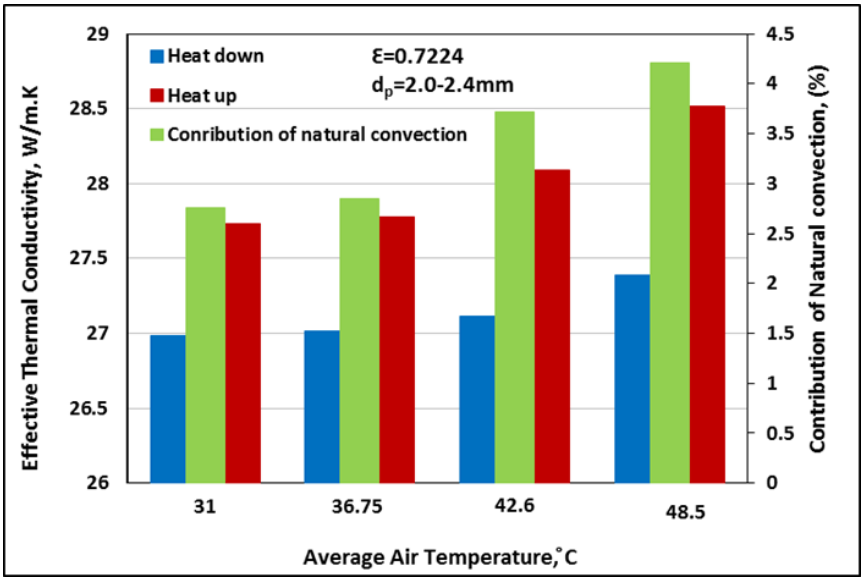

Figure 4. The impact of temperature on the contribution of natural convection to ETC

The dependence of sample properties on convection was explored by testing four large pore size samples (d_p = 2.0 - 2.4 mm) with different porosities in both upward and downward configurations. Shown in Figure 5 is the effect of porosity on the contribution of convective heat transfer to *ETC*, including data from a high porosity aluminium foam [9] whose pore size is roughly equivalent to the pore size tested here. The contribution of natural convection is calculated as the percentage increase in *ETC* when measured with heat flow vertically upwards, over the value when it flows in the opposite direction (suppressing the convection contribution), and is found to increase with porosity as a result of increased fluid space. However, the overall contribution from natural convection remains low. Subsequent measurements were performed with the direction of heat downwards to minimize influence of convective heat transfer.

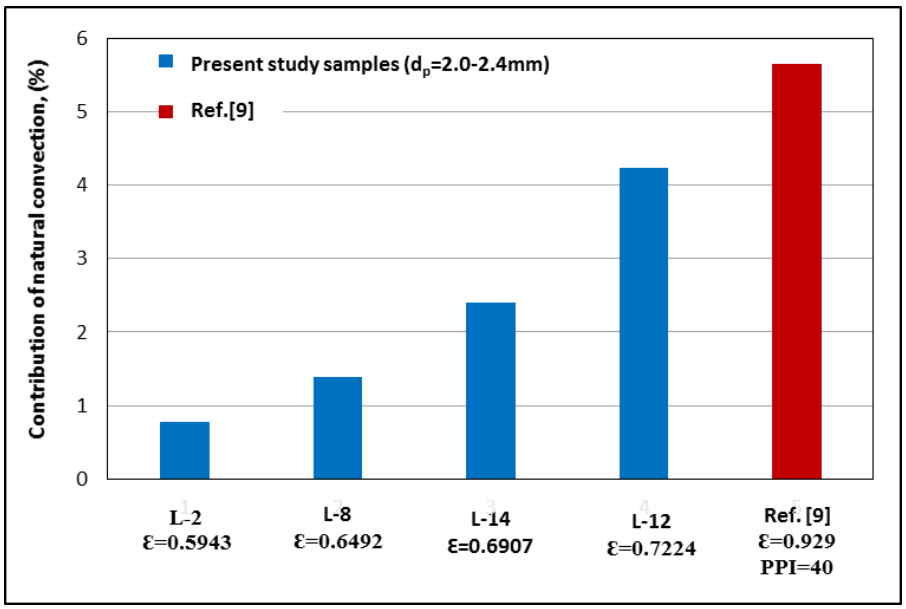

Figure 5. The effect of porosity on the natural convection contribution on ETC (33°C)

4. Uncertainty analysis

There are a number of measured parameters which lead to the main uncertainties in this experimental work. These parameters should be taken into account to estimate the errors in *ETC* and porosity. Porosity can be expressed as function of cross sectional area (A), length (L_s) and sample mass (m_s) of the sample:

$$\varepsilon = f(L_s, A, m_s) \tag{4.6}$$

The uncertainty of the porosity can be estimated [7, 14, 15, 35] as:

$$\frac{\delta\varepsilon}{\varepsilon} = \sqrt{\left(\frac{\delta A}{A}\right)^2 + \left(\frac{\delta L_s}{L_s}\right)^2 + \left(\frac{\delta m_s}{m_s}\right)^2} \tag{4.7}$$

The other important parameter is heat transfer and its uncertainty is function of the error in upper and lower heat flux meters (Q_I, Q_{II}), physical dimensions of the sample and temperature differences (ΔT) as:

$$Q_s = f(L_s, A, Q_I, Q_{II}, \Delta T) \tag{4.8}$$

Therefore, the uncertainty can be found as

$$\frac{\delta Q_s}{Q_s} = \sqrt{\left(\frac{\delta A}{A}\right)^2 + \left(\frac{\delta L_s}{L_s}\right)^2 + \left(\frac{\delta Q_I}{Q_I}\right)^2 + \left(\frac{\delta Q_{II}}{Q_{II}}\right)^2 + \left(\frac{\delta \Delta T}{\Delta T}\right)^2} \tag{4.9}$$

Considering the relation which used to calculate the effective thermal conductivity the related parameters can be expressed as follows:

$$K_{eff} = f(L_s, A, Q_s, \Delta T) \tag{4.10}$$

Then the uncertainty of the effective thermal conductivity can be as

$$\frac{\delta K_{eff}}{K_{eff}} = \sqrt{\left(\frac{\delta A}{A}\right)^2 + \left(\frac{\delta L_s}{L_s}\right)^2 + \left(\frac{\delta Q_s}{Q_s}\right)^2 + \left(\frac{\delta \Delta T}{\Delta T}\right)^2} \tag{4.11}$$

The uncertainties of parameters which were used in the valuation of effective thermal conductivity are given in Table 2. From the above calculation the

uncertainty of the porosity was found to be <1.8% and the uncertainty of the effective thermal conductivity was <6.1%.

Table 2 Parameters Uncertainties

Parameter	Uncertainty
Sample length (L_s)	0.4%
Sample Area (A)	0.8%
Sample Weight (m_s)	0.25%
Porosity (ε)	1.8%
Temperature Difference (ΔT)	0.25°C

5. Experimental Results:

Shown in Figure 6 are the measured effective thermal conductivities of tested samples plotted against porosity. There was some scatter in the results which is inherent from the nature of porous metals, the manufacturing process and the size of samples that could be manufactured.

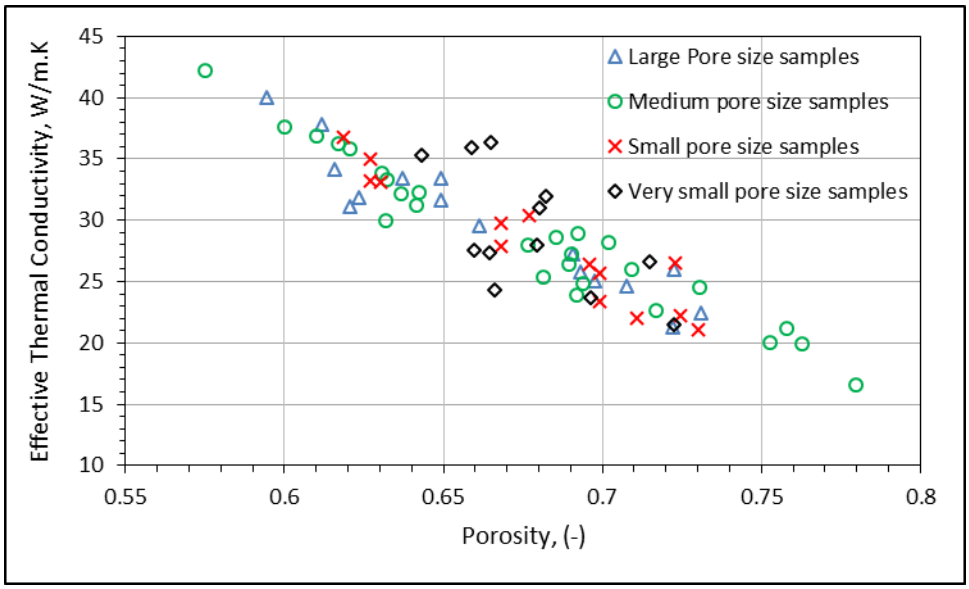

Figure 6. The effective thermal conductivity versus porosity (K_s=205 W/m.K, temperature is 33°C)

In order to compare the measured values of *ETC* with those available in the literature, *ETC* is presented (Figure 7) normalized with the thermal conductivity of solid material from which the porous structure is made. The results of other workers are also presented.

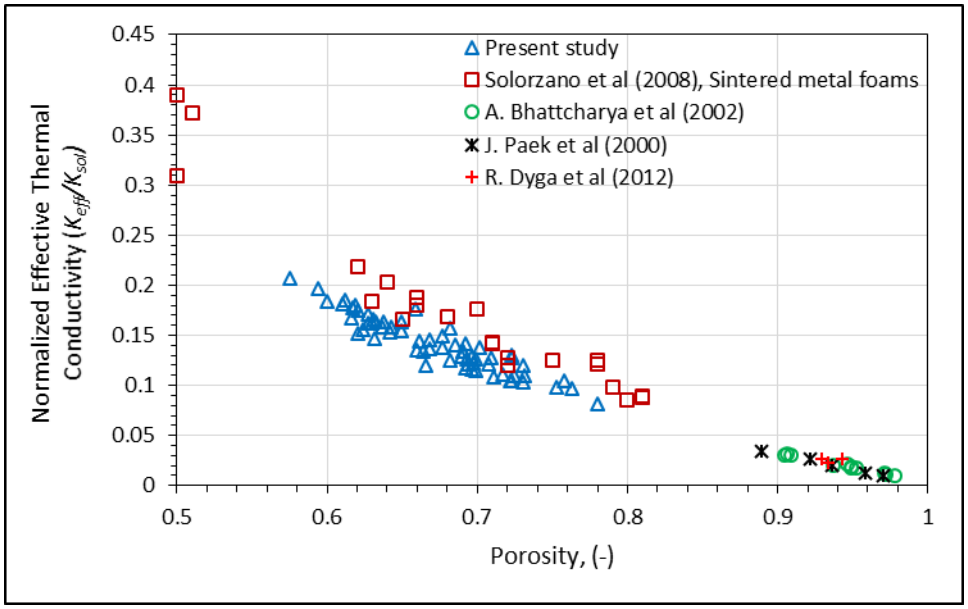

Figure 7 Normalized thermal conductivity versus porosity

It can be seen that for the samples tested here, and those of other workers, the *ETC* decreased as the porosity increased. The foams manufactured by Solórzano et al. by the powder metallurgical method resulted in closed cells with a similar range of porosities to those manufactured here. They used the Transient Plane Source (TPS) technique to determine *ETC*. Three representative measurements of high porosity metal foams manufactured using investment casting have been included. The samples tested in Paek et al[5] and Bhattacharya et al [15] are Duocel foams, produced by the ERG Materials and Aerospace Corp. Dyga and Witczak [9] do not mention the origin of their samples but are reported as ranging from 20 to 40 PPI. All used a similar method to determine *ETC* as the one used here.

The thermal conductivity of the air (fluid phase) was smaller than the aluminium (solid phase) hence the main mechanism of heat transfer was conduction through the ligaments of the metal network. Reducing the volume fraction of the fluid (decreasing porosity) increases the thickness of the struts (the elements of the solid skeleton) which form the unit cells resulting in higher values of *ETC*. For the range pore sizes typically found in these materials the size of the pores does not have an influence on *ETC*.

6. Validity with correlations and models

Since their development, there have been a number of studies on high porosity metal foams and sponges ($\varepsilon > 90\%$) in these *ETC* has been shown to be strongly influenced by the morphology of the unit cell [19]. Empirical and structural based models have been developed, however, theoretical models of

ETC often still rely on experimentally determined constants to account for manufacturing variability and the difficulties in representing the complex three dimensional structures [11, 19]. Models have often been based on a number of structures such as a two-dimensional array of hexagonal cells [6] and 3D tetrakaidecahedron cell[18, 28].

The materials studied here have lower porosities and a more random structure than some other types of porous material so their *ETC* would not necessarily be expected to agree with equations derived for alternative types of metal foam or sponge. However, it is desirable to have an expression that can predict *ETC* for porous metals over the range of porosities from 0.5 to values approaching 1.0. A number of models and correlations have been selected and compared to available measurements of *ETC*, which are given in Table 3. Three simplified models were used, one based on the assumption that conduction through the solid material can be either in series or parallel. A simple scaling expression was also used, along with the Dul'nev model [8, 15, 36], and an analytical model based on the numerical and 3D tomographic structure parameters in terms of ratio between the thickness of the struts and the nodes (referred to as lumps in the originating work, and preserved in the notation here, D_{st}/d_{lu}) and the node shape [18]. Two empirical expressions for high porosity (> 90%) foams are also compared to our experimental measurements. These are being applied beyond their proven range of applicability to observe if they might extend to lower porosity materials.

Table 3. Models and empirical correlations:

Name	Expression
Simplified models:	
Simplified Coquard et al. model [18]	$K_{eff} = \alpha\,(1-\varepsilon) + \chi(1-\varepsilon)^2$ $\alpha = f\left({}^{D_{st}}/_{d_{lu}}\right),\ \chi = f\left({}^{D_{st}}/_{d_{lu}}\right)$
Simplified Series – Parallel and Misnar Models [6]	$K_{eff} = K_s(1-\varepsilon^{2/3})$
Dul'nev Model [37]	$K_{eff} = K_s t^2 + K_f(1-t)^2 + \frac{2t(1-t)K_sK_f}{K_s(1-t)+tK_f}$ where $t = \frac{1}{2} + \cos\left(\frac{1}{3}cos^{-1}(2\varepsilon-1) + \frac{4\pi}{3}\right)$
Scaling Relation [6, 38]	$K_{eff} = K_s(1-\varepsilon)^n$ where $n \in [1.65, 1.85)$
Empirical Correlations for high porosity foams:	
Bhattacharya et al. [15]	$K_{eff} = A(\varepsilon K_f + (1-\varepsilon)K_s) + \frac{1+A}{\frac{\varepsilon}{K_f}+\frac{1-\varepsilon}{K_s}}$ where A= 0.35

Singh et al. [36]	$k_{eff} = K_I^{(1-F)} K_{II}^F \quad 0 \le F \le 1$ $K_I = \frac{K_s K_f}{(1-\varepsilon)K_f + \varepsilon K_s}$ $K_{II} = \varepsilon K_f + (1-\varepsilon)K_s$ $F = 0.9683\ (0.3031 + 0.0623 \ln(\varepsilon \frac{K_s}{K_f}))$

The selected correlations and models are plotted with experimental data (our own and that of other workers) in Figure 8.

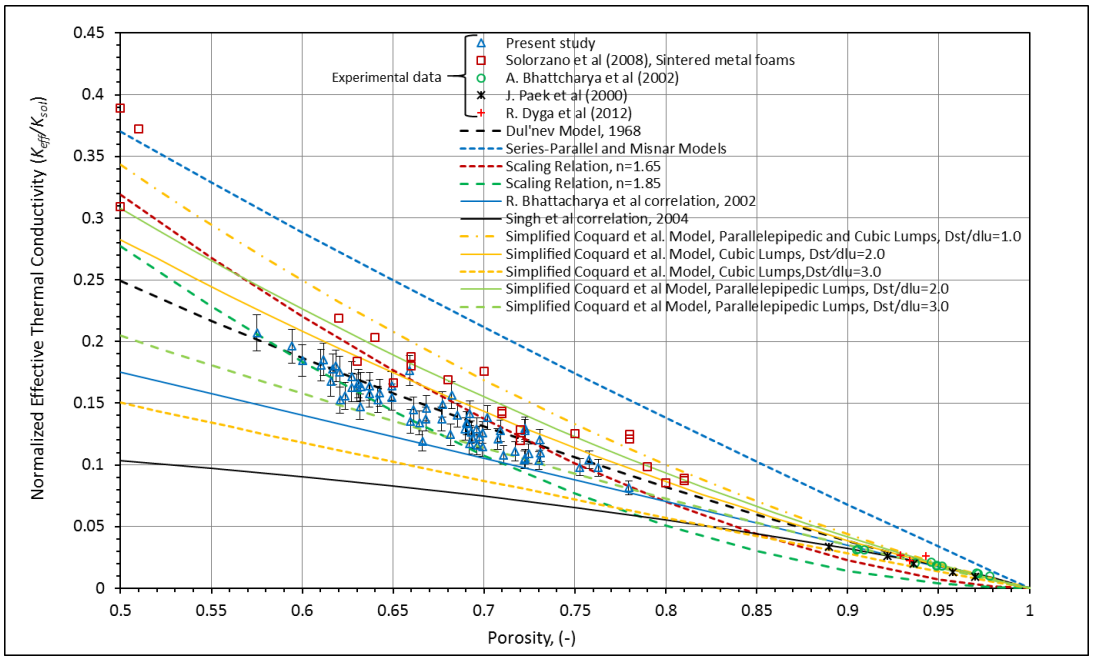

Figure 8 Empirical correlations and simplified models versus porosity.

From Figure 8 it can be seen that there is considerable variation in the predicted *ETC*, with mismatches between empirical correlations and the experimental results across the full range of porosity. The experimental data might be considered to be in better agreement than the proposed fits, the scatter observed between the samples tested here being less than that of the predictions. This, in part, reflects the lack of experimental data that has been available for porous materials and the necessity for further measurements. The series-parallel or Minsar models over predicted *ETC* at all porosities by 65% at a porosity of 70% and 86% at a porosity of 95%. The two models derived for high porosity materials, Bhattacharya et al.[15], and Singh et al.[36], tend to under predict *ETC at* lower porosities by 24% and 50% at a porosity of 60% respectively, indicating some material/structural difference in the materials at this range from the higher porosity form. Scaling relationships gave reasonable agreement for some of the measurements but tended not to

work for material where the porosity was greater than 90% where they under predicted *ETC* by 77% at a porosity of 95%. The Dul'nev model predicted *ETC* well across the whole range of porosities, although the values of the effective thermal conductivity for the high porosity foams are so low the relative error will be significant. The successful predictions of this model is likely to relate to the fact that the fibrous structure in the model is assumed to be an infinite random arrangement of cylinders. The replacement of the cylinders with square bars of the same cross sectional area will not affect *ETC* [37], and so this random arrangement is a good representation of the strut structure of the tested foams.

Further to this, the shapes of the nodes and struts have a measurable effect on the predicted *ETC*. The cross sectional shape of metal fibre (strut) changes with porosity, from a circle at a porosity of 85% to a concave triangle when the porosity reaches 97% [15, 21, 39]. To include the effect of the thickness ratio of the nodes and struts, the predicted *ETC* from the Coquard et al model [18] was compared with experimental results with cubic and parallelepipedic node shapes. For both shapes at high D_{st}/d_{lu} the *ETC* under predicted at low porosity by 15% and 36% for parallelepipedic and cubic nodes respectively, and tends to good estimation at very high porosities with high and low ratio. The overestimated values were found at lower porosities with very low D_{st}/d_{lu}. When the ratio is 2.0 the shape of the nodes tends to a measurable difference of around 8% at a porosity of 65%. In this model the thickness ratio between the nodes and struts needs to be obtained accurately in order to be able to predict a reliable *ETC* value.

The analytical and numerical approaches describe the typical shape of unit cells as homogenous, without any misalignment or other defects, which in reality will be common. Such features will be the origin of the differences between the predictions and the experimental results.

To further investigate the relationship between *ETC* and porosity an empirical scaling relationship was derived where:

$$K_{eff} = K_s(1-\varepsilon)^{n=f(\varepsilon)} \qquad 6.1$$

Such that *n* was itself a function of the porosity. It was initially anticipated that *n* would be a linear function. Shown in Figure 9 is the value of the exponent *n* plotted against porosity for each experimental data point. The measurements from this study and those of other workers presented in Figure 7 were used. The value of *n* was observed to gently decrease with increasing porosity but

then rapidly tail off beyond a porosity of 0.8. In order to fit these data a power law was investigated, also shown in Figure 9, as a dashed line. The best fit was found to be:

$$n = 2.15(1-\varepsilon)^{0.16} \qquad 6.2$$

Resulting in final form of the empirical scaling law for porous metals for with pore fractions ranging from 0.5 to 0.98 to be

$$K_{eff} = K_s(1-\varepsilon)^{2.15(1-\varepsilon)^{0.16}} \qquad 6.3$$

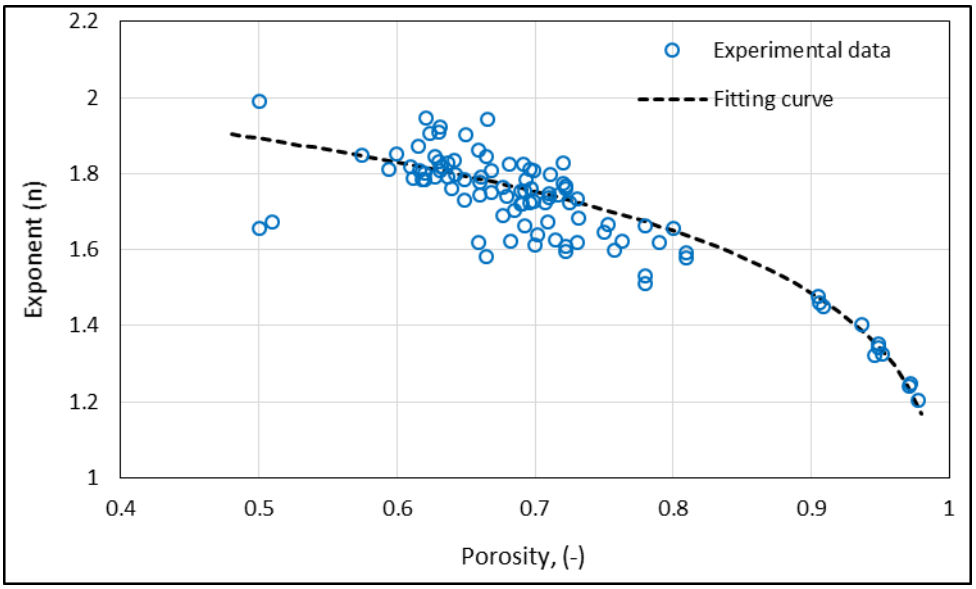

Figure 9. The exponent n from the proposed empirical scaling relationship as a function of porosity.

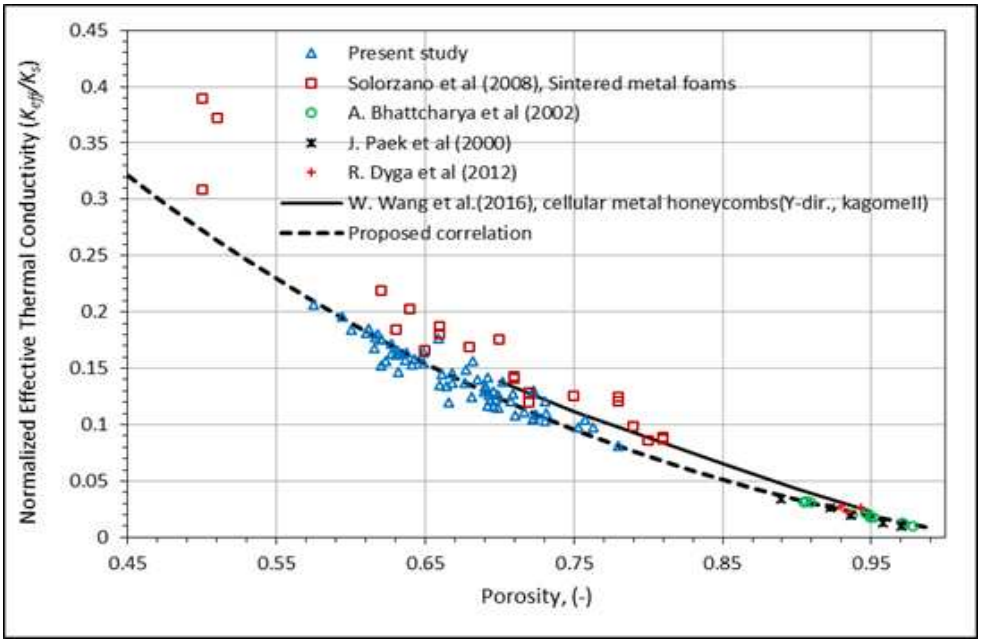

Figure 10 Predicted effective thermal conductivity by modified correlation versus porosity

Shown in Figure 10 are selected experimental data with the proposed empirically derived scaling law given in Equation 6.3. The agreement with all three forms of porous material is considered to be good. There is some deviation with the 'low' porosity sintered metal foams (which are closed cell) [6] which had slightly higher *ETC* than the open celled materials probably due to the structural difference. Also shown in Figure 10 is the prediction by an analytical expression for cellular metal honeycombs [40]. Here the thickness and height of the solid material decreases in proportion as the porosity increases i.e. the cells become smaller and the walls thinner. The reduction in effective thermal conductivity with porosity is more linear in this situation. It should be noted that these results are only applicable for unidirectional heat transfer and that there is a different correlation for heat transfer in alternative planes. In contrast the high porosity metal foams ($\varepsilon > 0.9$) are characterised by thickened intersections with thinner walls resulting in relatively lower values of *ETC* than might be expected if the material was distributed evenly in the matrix.

The empirical expression derived here clearly has its limitations, however, it provides better agreement with the full range of experimental data than the existing analytical expressions. While methods that make links between the structure and the behaviour clearly have great potential to yield understanding of the mechanisms and could lead to accurate predictions, accessing all of the required parameters experimentally can be challenging. Structural differences

inherent in the different manufacturing techniques (e.g. the thin strut thicknesses seen in the high porosity investment cast foams), and changes in structure over large ranges of porosity, mean that a general correlation for *ETC* will be difficult to achieve.

7. Conclusion

The effective thermal conductivity, *ETC*, of aluminium metal sponges manufactured using the replication technique were measured by a comparative steady state technique. The porosity ranged from 0.6 to 0.8 for four different pore sizes (~0.7 to 2.4 mm). The impact of thermal convection on the measurements was found by comparing the results for a heat flux acting with and against gravity. It is estimated that convection heat transfer might contribute up to 4% of the heat transfer through the samples.

The effective thermal conductivity was found to fall with increasing porosity. The measurements were similar to those of other workers for closed cell porous materials. Comparison of the results from this study and measurements of other workers with a selection of models and expressions for the effective thermal conduction showed that the equation proposed by Dul'nev gave the best prediction for porosities ranging from 0.5 to 1.0. However, the effective thermal conductivity was so small at high porosities (greater than 90%) that the relative error is high for these samples. An empirical correlation was proposed for the effective thermal conductivity from 0.5 to 1.0 based on a scaling law with the exponent a function of the porosity. This is proposed as a pragmatic solution to the variation in the material structure and properties resulting in difficulties to develop an analytical expression.

Acknowledgment

One of the authors (EMEL) would like to acknowledge the Mexican Government's National Council of Science and Technology CONACYT for provision of a scholarship. The work received no other financial support.

1. Goodall, R. and A. Mortensen, *24 - Porous Metals A2 - Laughlin, David E*, in *Physical Metallurgy (Fifth Edition)*, K. Hono, Editor. 2014, Elsevier: Oxford. p. 2399-2595.

2. *Index A2 - Laughlin, David E*, in *Physical Metallurgy (Fifth Edition)*, K. Hono, Editor. 2014, Elsevier: Oxford. p. 2837-2899.
3. Mortensen, R.G.A., *Porous Metals*, in *Physical Metallurgy*. 2014, Elsevier. p. 2399-2595.
4. Mancin, S., L. Rossetto, and Iop. *An assessment on forced convection in metal foams*. in *6th European Thermal Sciences Conference (Eurotherm)*. 2012. Poitiers, FRANCE: Iop Publishing Ltd.
5. Paek, J.W., et al., *Effective thermal conductivity and permeability of aluminum foam materials.* International Journal of Thermophysics, 2000. **21**(2): p. 453-464.
6. Solorzano, E., et al., *An experimental study on the thermal conductivity of aluminium foams by using the transient plane source method.* International Journal of Heat and Mass Transfer, 2008. **51**(25-26): p. 6259-6267.
7. Zhao, C.Y., et al., *The temperature dependence of effective thermal conductivity of open-celled steel alloy foams.* Materials Science and Engineering: A, 2004. **367**(1–2): p. 123-131.
8. Calmidi, V.V. and R.L. Mahajan, *The effective thermal conductivity of high porosity fibrous metal foams.* Journal of Heat Transfer-Transactions of the Asme, 1999. **121**(2): p. 466-471.
9. Dyga, R. and S. Witczak. *Investigation of effective thermal conductivity aluminum foams*. in *Procedia Engineering*. 2012.
10. Mendes, M.A.A., et al., *Experimental validation of simplified conduction-radiation models for evaluation of Effective Thermal Conductivity of open-cell metal foams at high temperatures.* International Journal of Heat and Mass Transfer, 2014. **78**: p. 112-120.
11. Ranut, P. and E. Nobile, *On the effective thermal conductivity of metal foams.* Journal of Physics: Conference Series, 2014. **547**(1).
12. Mendes, M.A., et al., *Measurement and simplified numerical prediction of effective thermal conductivity of open-cell ceramic foams at high temperature.* International Journal of Heat and Mass Transfer, 2016. **102**: p. 396-406.
13. Ye, H., M. Ma, and Q. Ni, *An experimental study on mid-high temperature effective thermal conductivity of the closed-cell aluminum foam.* Applied Thermal Engineering, 2015. **77**: p. 127-133.
14. Sadeghi, E., S. Hsieh, and M. Bahrami. *Thermal contact resistance at a metal foam-solid surface interface*. in *ASME/JSME 2011 8th Thermal Engineering Joint Conference, AJTEC 2011*. 2011.
15. Bhattacharya, A., V.V. Calmidi, and R.L. Mahajan, *Thermophysical properties of high porosity metal foams.* International Journal of Heat and Mass Transfer, 2002. **45**(5): p. 1017-1031.
16. Skochdopole, R.E., *The Thermal Conductivity of Foamed Plastics. Chemical Engineering Progress*, 1961(55:57): p. 10.
17. *Copyright of Volume I A2 - Laughlin, David E*, in *Physical Metallurgy (Fifth Edition)*, K. Hono, Editor. 2014, Elsevier: Oxford. p. iv.
18. Coquard, R., D. Rochais, and D. Baillis, *Conductive and radiative heat transfer in ceramic and metal foams at fire temperatures.* Fire technology, 2012. **48**(3): p. 699-732.
19. Yang, X., et al., *A simplistic analytical unit cell based model for the effective thermal conductivity of high porosity open-cell metal foams.* J. Phys. D-Appl. Phys., 2013. **46**(25).
20. Mendes, M.A.A., S. Ray, and D. Trimis, *An improved model for the effective thermal conductivity of open-cell porous foams.* International Journal of Heat and Mass Transfer, 2014. **75**: p. 224-230.
21. Kumar, P., F. Topin, and J. Vicente, *Determination of effective thermal conductivity from geometrical properties: Application to open cell foams.* International Journal of Thermal Sciences, 2014. **81**(0): p. 13-28.
22. Coquard, R., D. Rochais, and D. Baillis, *Experimental investigations of the coupled conductive and radiative heat transfer in metallic/ceramic foams.* International Journal of Heat and Mass Transfer, 2009. **52**(21): p. 4907-4918.

23. Laschet, G., et al., *Effective permeability and thermal conductivity of open-cell metallic foams via homogenization on a microstructure model.* Computational Materials Science, 2009. **45**(3): p. 597-603.
24. Gustafsson, S.E., E. Karawacki, and M.N. Khan, *Transient hot-strip method for simultaneously measuring thermal conductivity and thermal diffusivity of solids and fluids.* Journal of Physics D: Applied Physics, 1979. **12**(9): p. 1411.
25. Gustafsson, S.E., *Transient plane source techniques for thermal conductivity and thermal diffusivity measurements of solid materials.* Review of scientific instruments, 1991. **62**(3): p. 797-804.
26. Gustafsson, S., *A device for measuring thermal properties of a sample of a substance*. 1989, Google Patents.
27. Thewsey, D. and Y. Zhao, *Thermal conductivity of porous copper manufactured by the lost carbonate sintering process.* PHYSICA STATUS SOLIDI A APPLICATIONS AND MATERIALS SCIENCE, 2008. **205**(5): p. 1126.
28. Goodall, R. and A. Mortensen, *Microcellular Aluminium? – Child's Play!* Advanced Engineering Materials, 2007. **9**(11): p. 951-954.
29. Elizondo Luna, E.M., et al., *Casting protocols for the production of open cell aluminum foams by the replication technique and the effect on porosity.* Journal of visualized experiments : JoVE, 2014(94).
30. Holman, J.P., *Heat transfer*. 10th ed. ed. 2010, Boston: Boston : McGraw Hill Higher Education, c2010.
31. Mancin, S., et al., *Pressure drop during air flow in aluminum foams.* International Journal of Heat and Mass Transfer, 2010. **53**(15-16): p. 3121-3130.
32. Lacroix, M., et al., *Pressure drop measurements and modeling on SiC foams.* Chemical Engineering Science, 2007. **62**(12): p. 3259-3267.
33. Klempner, D. and K.C. Frisch, *Handbook of polymeric foams and foam technology*. Vol. 404. 1991: Hanser Munich etc.
34. Sadeghi, E., S. Hsieh, and M. Bahrami, *Thermal conductivity and contact resistance of metal foams.* Journal of Physics D: Applied Physics, 2011. **44**(12): p. 125406.
35. John, R.T., *An introduction to error analysis : the study of uncertainties in physical measurements*. 2nd ed. ed. 1997, Sausalito, Calif.: Sausalito, Calif. : University Science Books, c1997.
36. Singh, R. and H.S. Kasana, *Computational aspects of effective thermal conductivity of highly porous metal foams.* Applied Thermal Engineering, 2004. **24**(13): p. 1841-1849.
37. Dul'nev, G.N. and B.L. Muratova, *Thermal conductivity of fibrous systems.* Journal of Engineering Physics, 1972. **14**(1): p. 15-18.
38. Ashby, M., et al., *Metal Foams: A Design Guide.* Applied Mechanics Reviews, 2001. **54**(6): p. B105.
39. Ranut, P., E. Nobile, and L. Mancini, *High resolution microtomography-based CFD simulation of flow and heat transfer in aluminum metal foams.* Applied Thermal Engineering, 2014. **69**(1–2): p. 230-240.
40. Wang, W., et al., *Analytical design of effective thermal conductivity for fluid-saturated prismatic cellular metal honeycombs*. 2016. p. 69-75.